ON THE TIME EVOLUTION OF THE LOCAL FLOW TOPOLOGY IN A TURBULENT BOUNDARY LAYER

G.E. Elsinga* and **I. Marusic**
Department of Mechanical Engineering,
The University of Melbourne
Victoria 3010, Australia
g.e.elsinga@tudelft.nl
imarusic@unimelb.edu.au

*present address: Laboratory for Aero and Hydrodynamics, Delft University of Technology

ABSTRACT

The average rates of change of the invariants of the velocity gradient tensor (Q and R) have been determined experimentally in the outer layer of a turbulent boundary layer as a function of the invariants themselves. Subsequent integration yields trajectories in the QR plane describing the average evolution of the local flow topology following a fluid particle. The trajectories reveal inward spiralling orbits around and converging to the origin. The orbit's period is nearly constant at $14.3\delta/U_e$, which may be regarded as the characteristic lifetime of the energy containing eddies in this part of the boundary layer. Furthermore, an empirical model for the average Q and R evolution is presented that reproduces the main features of the orbits in the vicinity of the origin.

1. INTRODUCTION

Turbulence is not a purely random phenomenon, but instead is well known to contain topological flow structures that are coherent in time and space, commonly referred to as eddies or coherent structures (Cantwell 1981). They are fundamental to our present understanding of turbulence and consequently, in relation to turbulent boundary layers, the instantaneous spatial organization of the eddies in hairpin vortices, packets and very-large-scale motions has recently received important attention (see Adrian 2007 for a review), leaving, however, open questions regarding the dynamics and time-scales of these eddies.

In this study we provide a first step in that direction by describing experimental findings on the average evolution of the local flow topology in a turbulent boundary layer. In this evolution two time scales are observed related to changing topology by eddy interactions and to decaying topology by viscous diffusion respectively.

For a non-rotating flow such as the turbulent boundary layer, the local topology in each point at each time instant can be classified based on an evaluation of the velocity gradient tensor $A = \nabla V$ as outlined in Chong et al. (1990). In that study it was further shown that for an incompressible flow, the generalized topology depends solely on the second and the third invariant of this tensor, Q and R, which are given by:

$$Q = -\frac{1}{2}A_{ij}A_{ji}$$
$$R = -\frac{1}{3}A_{ij}A_{jk}A_{ki} \qquad (1)$$

The first invariant, $P = -A_{ii}$, is identically zero because of continuity. Hence the evolution of the flow topology in the present boundary layer can be described by the development of Q and R in time.

The four main local topology classes are summarized in the QR phase plane in figure 1. Above the null discriminant line (i.e. $D = R^2/4 + Q^3/27 = 0$) the flow pattern is focal, while below this curve it is non-focal or node/saddle. Further subdivision into so-called stable and unstable flow patterns is based on the sign of R. For a more complete discussion of these local topologies is referred to Chong et al. (1990) and Perry and Chong (1987).

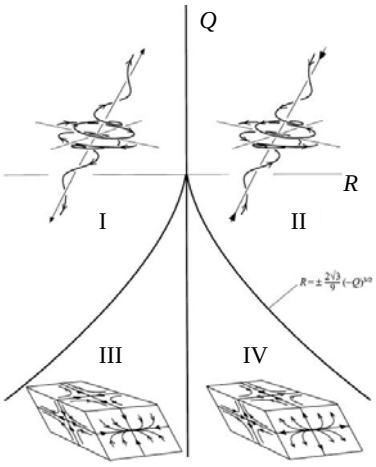

Figure 1: Local flow topologies associated with the invariants of the velocity gradient tensor (Q and R) for incompressible flow. (taken from Ooi et al. 1999)
I: stable focus/stretching,
II: unstable focus/compressing,
III: stable node/saddle/saddle,
IV: unstable node/saddle/saddle.

In the past investigations of the local flow topology in turbulence were almost exclusive to Direct Numerical Simulations (DNS, e.g. Cantwell 1993, Soria et al. 1994, Chong et al. 1998) or analytical methods (e.g. Cantwell 1992), because they require all three components of velocity as well as their spatial derivatives to evaluate the invariants of velocity gradient tensor Q and R. Even with temporal information accessible, most of these studies are restricted to a description of the instantaneous flow. A procedure to investigate the average dynamic behaviour of the invariants was proposed by Martin et al. (1998) and Ooi et al. (1999), who studied the conditional average evolution of the local topology in DNS of isotropic turbulence and showed that these topology evolutions describe spiralling orbits in the QR space and tend to converge to a point (i.e. the origin).

Here this approach is extended to the larger scales of motion in the outer layer of a turbulent boundary layer (> 50 viscous length scales) to establish characteristic life-times for the large energy containing eddies. Through a comparison with DNS data some potentially universal aspects of the local flow topology dynamics across the range of scales and the different turbulent flows may be identified, as well as the differences.

One of the novel aspects of the present study is the experimental approach enabled by recent advances in velocimetry methods, in particular Tomographic Particle Image Velocimetry (Elsinga et al. 2006). It is an extension of standard planar PIV capable of instantaneously measuring all three components of velocity in a 3D volume, which allows an assessment of the velocity gradient tensor. The method can be extended even further to three-dimensional time-resolved measurements by using high repetition rate PIV hardware (Schröder et al. 2008a).

In the remainder of the paper, the experimental dataset is introduced (section 2) and the instantaneous joint-pdf of the invariants of the velocity gradient tensor is discussed (section 3). Then the method to obtain the average dynamics of the invariants will be presented in section 4 with results. From the substitution of these results in the Navier-Stokes equations rewritten in terms of the velocity gradient tensor (section 5), the average effect of the eddy interactions can be inferred, which will also lead to the formulation of an empirical model for the dynamics of Q and R (section 6). Section 7 then summarizes the conclusions.

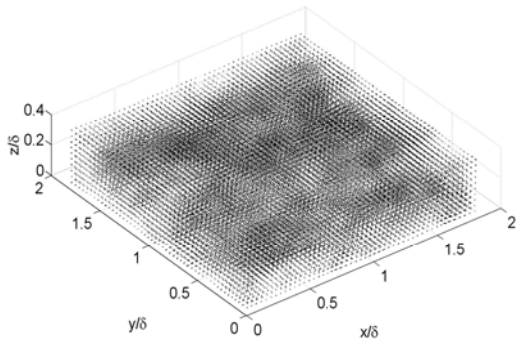

Figure 2: Example of an instantaneous velocity field measured with time-resolved tomographic-PIV relative the volume average velocity. Only every other vector is plotted.

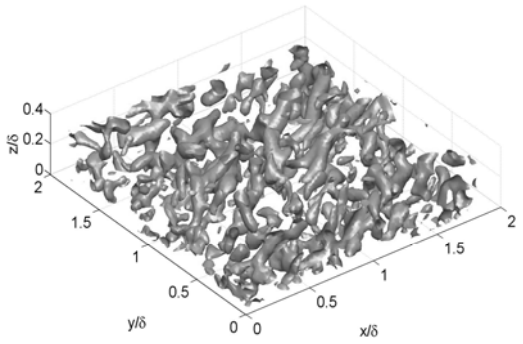

Figure 3: Iso-surface of constant Q in the instantaneous velocity distribution of figure 2 (displayed level: $Q/\langle Q_W \rangle = 0.9$).

2. EXPERIMENTAL DATASET

The zero-pressure gradient turbulent boundary layer data used in this investigation has been obtained from a time-resolved tomographic PIV experiment in the water tunnel of the Aero & Hydrodynamics Laboratories of TU Delft. The setup and first results of this collaborative effort between TU Delft Aerospace Engineering and Mechanical Engineering Aerodynamics Laboratories, DLR Göttingen and LaVision GmbH have been described in Schröder et al. (2008b). For completeness, however, we will briefly recall some of the boundary layer properties here. The boundary layer develops over a 2.5 m long flat plate with an elliptical leading edge at a free-stream flow velocity U_e of 0.53 m/s. Transition is imposed 15 cm downstream of the elliptical leading edge by a zig-zag strip. At the measurement location, 2.0 m downstream, the boundary layer thickness δ is 37 mm and the Reynolds numbers Re_θ and Re_τ are 2460 and 800 respectively.

The three dimensional velocity distribution $\vec{V}(x,y,z,t)$ is evaluated in a volume spanning $1.8\delta \times 1.8\delta$ in streamwise, x, and spanwise, y, direction and covering $z/\delta \in [0.11 , 0.30]$ in wall-normal (z) direction over a period of 2 seconds. The sampling frequency is 1 kHz (corresponding to $70U_e/\delta$). A typical example of the instantaneous vector field is presented in figure 2. The spatial resolution, taken as the cross-correlation volume dimension, is 0.07δ corresponding to approximately 50 viscous length scales in each direction. Between subsequent velocity volumes in time, the flow structures advect by approximately 10 viscous length scales.

The measured velocity fields correspond to the large energy-containing eddies, as can be seen from the pre-multiplied velocity power spectra presented for example in Balakumar and Adrian (2007) and Hutchins and Marusic (2007). In the measurement, wavenumbers $k < 50/\delta$ are resolved, which, at the present Reynolds number, contain over 96% of the turbulent kinetic energy associated to the streamwise velocity component. Similar values were shown for the Reynolds shear stress (Balakumar and Adrian 2007).

3. INSTANTANEOUS DISTRIBUTION OF THE INVARIANTS OF THE VELOCITY GRADIENT TENSOR

As a starting point for the discussion of the time evolution, we first consider the instantaneous distribution of the invariants. An iso-surface of a constant positive Q, as determined from the instantaneous velocity field of figure 2, is shown in figure 3. Plots like this visualize regions with a focal topology and have been used frequently in the past to detect vortices. A statistical description of the volume and time average distribution of Q and R is given by their joint-PDF in figure 4, where the invariants are normalized using $\langle Q_W \rangle$, the average of the second invariant of the rate of rotation tensor (following Ooi et al. 1999). The contour lines exhibit the self-similar 'tear drop' shape around the origin that has also been observed in DNS studies of mixing layers, isotropic turbulence, channel and boundary layer flow (Soria et al. 1994, Ooi et al. 1999, Blackburn et al. 1996 and Chong et al. 1998). The similarity in these plots across the different flow cases has even inspired some speculation about a kind of universality in the invariant space of tubulence (Ooi et al. 1999). Moreover, the favourable comparison between limited spatial resolution PIV and fully resolved DNS may further suggest that this extends beyond the smallest scales of motion. The potential of universality may therefore render a further statistical description of the evolution of turbulent structure in terms of Q and R very attractive.

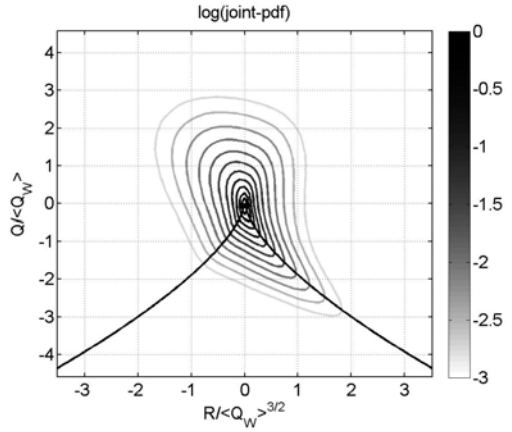

Figure 4: Normalized joint PDF of Q and R on a logarithmic scale. The black solid line indicates points for which the discriminant of the velocity gradient tensor equals zero.

4. DYNAMICS OF THE INVARIANTS

The dynamics of the invariants is investigated in a Lagrangian frame of reference moving with a fluid particle by means of their material derivatives, which are given by:

$$\frac{DQ}{Dt} = \frac{\partial Q}{\partial t} + u\frac{\partial Q}{\partial x} + v\frac{\partial Q}{\partial y} + w\frac{\partial Q}{\partial z}$$
$$\frac{DR}{Dt} = \frac{\partial R}{\partial t} + u\frac{\partial R}{\partial x} + v\frac{\partial R}{\partial y} + w\frac{\partial R}{\partial z} \qquad (2)$$

Note that all the terms on the right hand side depend only on the velocity $\vec{V}(x,y,z,t)$, hence Eq. 2 can be evaluated directly for the present dataset without further assumptions. Additionally, a conditional averaging technique is employed to obtain the mean temporal rate of change of the invariants Q and R as a function of invariants themselves. The averaging procedure is identical to the one of Ooi et al. (1999) and reads as:

$$\left\langle \frac{DQ}{Dt} \right\rangle (Q_0, R_0) =$$
$$\left\langle \frac{DQ}{Dt} \middle| -\Delta Q/2 \le (Q - Q_0) < \Delta Q/2 ; -\Delta R/2 \le (R - R_0) < \Delta R/2 \right\rangle$$

$$\left\langle \frac{DR}{Dt} \right\rangle (Q_0, R_0) =$$
$$\left\langle \frac{DR}{Dt} \middle| -\Delta Q/2 \le (Q - Q_0) < \Delta Q/2 ; -\Delta R/2 \le (R - R_0) < \Delta R/2 \right\rangle \qquad (3)$$

where Q_0 and R_0 are the bin centers and ΔQ and ΔR define the bin size over which the material derivative is averaged. Their respective values are $0.18\langle Q_W \rangle$ and $0.088\langle Q_W \rangle^{3/2}$. The result is presented in figure 5 as a vector field in the QR plane. The magnitude of the mean rate of change of Q and R (proportional to the vector length) increases with increasing distance from the origin. However, along the $R > 0$ part of the null discriminant curve (black solid line) the vector magnitude remains relatively small. These results are consistent with DNS of isotropic turbulence (Martin et al. 1998, Ooi et al. 1999).

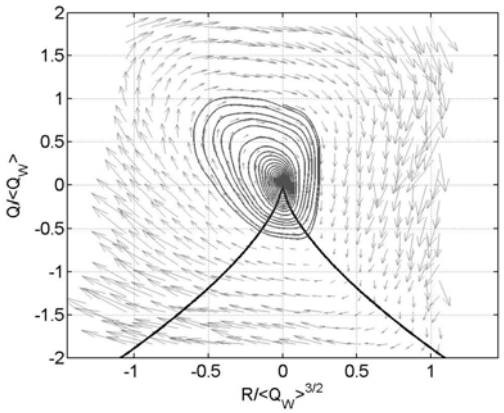

Figure 5: Conditional averaged rate of change of Q and R, i.e. vectors of DQ/Dt and DR/Dt, and a corresponding QR-trajectory (spiralling solid line).

The conditional average rate of change field can be integrated, which produces a QR trajectory as shown on top of the vectors in figure 5. The trajectory orbits around the origin in clockwise direction and spirals inwards. So, on average, the flow topology around a fluid particle changes cyclically from unstable focus, unstable node/saddle, stable node/saddle to stable focus (see figure 1). The values of Q, R and the discriminant D along the trajectory are plotted versus integration time in figure 6 each revealing a decrease with time corresponding to decreasing velocity gradients. Furthermore, the period of each orbit is found to be nearly constant at 1.00 seconds, corresponding to $14.3\delta/U_e$ or $10.4\langle Q_W \rangle^{-1/2}$, which may be regarded as a characteristic life-cycle-time of the eddies in this region of the boundary

layer ($0.11 < z/\delta < 0.30$; $88 < z^+ < 240$, corresponding normally to the outer region, including part of the logarithmic region). The period is surprisingly close to the estimated eddy-turnover time for the large scale eddies $\delta/u_{rms} = 14\ \delta/U_e$, where the rms velocity is taken at the center of the measurement volume. The wavelength associated to the orbits period is approximately 11 δ (using the average velocity in the volume 0.80 U_e as the convective velocity). This corresponds well with the location where a peak appears in the pre-multiplied power spectra of the streamwise component of velocity in wall-bounded turbulence. Balakumar and Adrian (2007) and Hutchins and Marusic (2007) have linked that peak to the very large-scale motions or superstructures observed in wall turbulence.

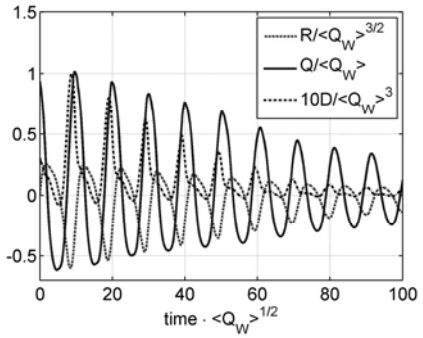

Figure 6: Time evolution of Q, R and the discriminant D along the conditional average trajectory shown in figure 5.

Additionally, a second time scale may be defined that is representative of the invariants average decay rate over the cycles. The decay, resulting in the inward spiral, is associated to viscous diffusion as shown in Martin et al. (1998) (see their figure 14). Diffusion increases with increasing velocity gradients, hence magnitude of Q and R, which is consistent with the reduced decay rate near the origin and the orbits being more closely spaced there (figure 5). Furthermore, the estimated diffusion time scale is $L^2/\nu = 300\delta/U_e$, where $L = 0.13\delta$ is a representative length scale (taken as the smallest resolved wavelength). This shows diffusion acts on times an order of magnitude larger than the orbit's period, which is again consisted with the trajectory in figure 5. Based on the difference in magnitude we regard the orbit's period as the relevant topology lifetime dictated by the eddy interactions. (Note that ignoring the eddy interactions through both the pressure and viscous forces results in a completely different, non-periodic evolution of the invariants [Cantwell 1993, Martin et al. 1998, Ooi et al. 1999].)

The orbit's period here is different from the DNS of Martin et al. (1998) for isotropic turbulence, who report a period of 3 eddy-turnover times, equivalent to $15\langle Q_W\rangle^{-1/2}$ in their case. The discrepancy may be explained by the difference in the flow scales investigated (small-scale in DNS and larger-scale presently). These differences become even more apparent when comparing the percentages of the orbit's period spent in each of the four topological states (table 1). For the large-scale motions in the present turbulent boundary layer (TBL) the average fluid particle spends relatively more time in a focal topology: 77 % compared to 42 % of the orbit in the DNS. This time is split almost equally between the stable and unstable focus in both studies. Another profound difference is found for the unstable node part of the orbit: 15 % (TBL) against 53 % (DNS), which must be related to the magnitude of the rates of change of the invariants being larger for the present large-scale motions. As a result the orbit's period decreases and the trajectory will not remain as long near the positive R branch of the null-discriminant curve. This part of the QR space has previously been associated to high rates of kinetic energy dissipation (Cantwell 1993), which is typically a small-scale phenomenon. This region is therefore likely to display differences.

Martin et al. (1998) also report that the trajectories are not perfectly self-similar especially the region corresponding to the nodal topologies. This suggests a dependence of the distance of the trajectory from the origin. Hence an additional explanation for the observed differences in the trajectories, which cannot be ruled out, is given by the present trajectories being chosen closer to the origin.

Table 1: Percentage of the time the QR trajectories spent in each of the topologies as indicated in figure 1 for the large-scale motion in turbulent boundary layer (TBL) and isotropic turbulence (DNS of Martin et al. 1998).

topology	TBL	DNS
I: stable focus	39 %	22 %
II: unstable focus	38 %	20 %
III: stable node	8 %	6 %
IV: unstable node	15 %	53 %

5. ANALYTICAL EXPRESSIONS

The obtained average rate of change can furthermore be inserted in the analytical expressions for the time evolution of the invariants as derived from the Navier-Stokes equations in Cantwell (1992). Conditional averaging these expressions results in:

$$\left\langle \frac{DQ}{Dt} \right\rangle (Q_0,R_0) = -3R_0 - \left\langle A_{ik}H_{ki} \right\rangle = -3R_0 - h_Q(Q_0,R_0)$$
$$\left\langle \frac{DR}{Dt} \right\rangle (Q_0,R_0) = \tfrac{2}{3}Q_0{}^2 - \left\langle A_{in}A_{nm}H_{mi} \right\rangle = \tfrac{2}{3}Q_0{}^2 - h_R(Q_0,R_0) \quad (4)$$

with

$$H_{ij} = -\left(\frac{\partial^2 p}{\partial x_i \partial x_j} - \frac{\partial^2 p}{\partial x_k \partial x_k}\frac{\delta_{ij}}{3} \right) + \nu \frac{\partial^2 A_{ij}}{\partial x_k \partial x_k} \quad (5)$$

where δ_{ij} is the Kronecker delta and A_{ij} is again the velocity gradient tensor, $A_{ij} = \partial u_i/\partial x_j$. The right hand side of Eq. 4 is composed of a contribution from local topology through Q and R and a non-local contribution through the tensor H_{ij} accounting for the interaction of adjacent fluid particles through pressure and viscous forces, which depends on the

position of the other eddies relative to the considered point the flow. Hence the latter term will not be a unique function of local flow quantities such as Q and R. Consequently the adopted conditional averaging procedure yields the average effect of these eddy interactions.

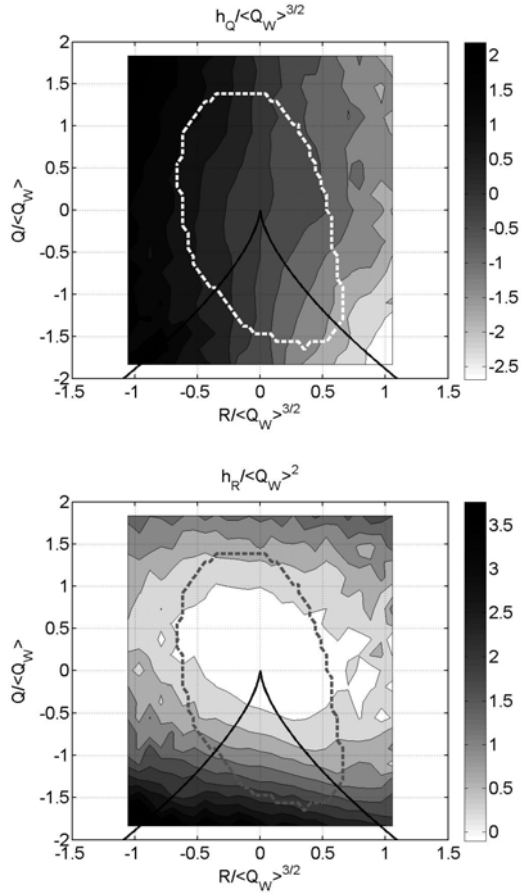

Figure 7: Contour plots of the h_Q (left) and h_R (right) terms in Eq. 4, which relate to the contribution of the eddy interactions to the conditional averaged rate of change of Q and R respectively. The dashed line indicates the region where the number of samples in each bin exceeds $5{\cdot}10^5$.

To see the contribution of the eddy interactions, the h_Q and h_R terms in Eq. 4 are computed and presented in normalized from in figure 7. Again the results reveal a good qualitative agreement with those obtained by DNS of isotropic turbulence (Martin et al. 1998), although only a more detailed view of the region near the origin is presented here. Furthermore, there appears to be a greater asymmetry in h_R in the Q direction in the present data consistent with the shorter time period the QR trajectories spend in the unstable node region, as mentioned above. From figure 7, it can also be seen that these h_Q and h_R terms are significant and are of the same order as the other right-hand-side terms in the invariants evolution equations, i.e. compare $-3R$ and $2/3Q^2$ along the coordinate axis with the contour levels. The sign of $-h_Q$ is predominantly opposite to $-3R$ hence has the effect of reducing DQ/Dt with respect to the inviscid, restricted Eulerian case ($H_{ij} = 0$, Cantwell 1992). Similarly, $-h_R$ has the effect of reducing DR/Dt, so the pressure and viscous forces act to reduce the average rate of change of the invariants. Furthermore, the magnitude of h_R is larger than $2/3Q^2$ for negative Q causing DR/Dt to become negative in that region, which consequently results in the observed spiralling QR trajectories. Hence, unstable nodes on average develop into stable nodes. Additionally, the pressure and viscous forces allow focal topologies to develop into nodal topologies and vice versa as opposed to the restricted Eulerian case where focal and nodal topologies remain so indefinitely (Cantwell 1992).

6. AN EMPIRICAL MODEL

The above results are synthesized by fitting relatively simple functions to h_Q and h_R thereby producing an empirical model for these terms. Note that only data enclosed by the dashed line in figure 7 will be used as the bins outside this region contain insufficient samples for convergence. Based on the contours in figure 7 a first order polynomial in Q and R is selected to approximate h_Q, while a second order polynomial is used for h_R. The polynomial coefficients are obtained from a least squares regression resulting in the following simple model:

$$\frac{h_Q}{\langle Q_w \rangle^{3/2}} = a_1 R^* + a_2 Q^* + a_3 R^* Q^* + a_4 R^{*2} + a_5 Q^{*2}$$

$$\frac{h_R}{\langle Q_w \rangle^{2}} = b_1 R^* + b_2 Q^* \qquad (6)$$

with

$$Q^* = \frac{Q}{\langle Q_w \rangle} \quad ; \quad R^* = \frac{R}{\langle Q_w \rangle^{3/2}} \qquad (7)$$

and where

$$a_1 = -0.165 \quad ; \quad a_2 = -0.318$$
$$a_3 = 0.428 \quad ; \quad a_4 = 0.475 \quad ; \quad a_5 = 0.663 \qquad (8)$$
$$b_1 = -1.859 \quad ; \quad b_2 = 0.213$$

Inserting these functions in Eq. 3 returns a set of differential equations for a dynamical system of two variables, which can then be solved. The mean rate of change of Q and R is presented in figure 8 with trajectories. The dashed trajectory is a separatrix, above which the trajectories spiral inwards as before. However, below this line the trajectories go to infinity, which is believed to be unphysical. Hence the model can be applied with confidence only inside the fitted region (marked by the dashed line in figure 7). Moreover, important differences between the model and the actual h_Q and h_R have been observed near the null discriminant curve and for large positive R strongly suggesting additional terms will be required for improved accuracy and extrapolation later on. Determining the nature of these additional terms would require either theory or converged data over a larger area in the QR space, but preferably both.

Nevertheless, near the origin the trajectories (the solid line in figure 8) reproduce the basic features of the measurement, such as the clockwise spiralling orbit, the deceasing value of the invariants with time and the

convergence to the origin. Even the orbit's period, 1.1 s corresponding to $16\delta/U_e$ and $11\langle Q_W\rangle^{-1/2}$, is in reasonable agreement (within 10%), so that the model may be regarded as a starting point for future refinements.

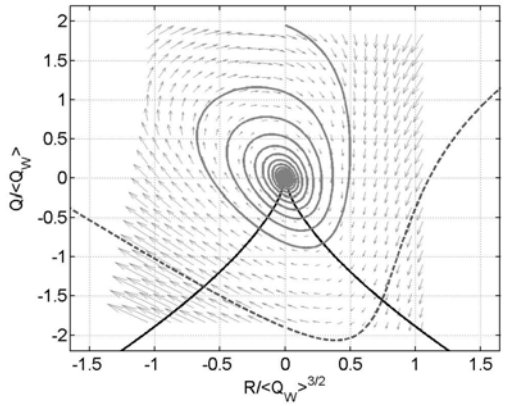

Figure 8: Empirical model for DQ/Dt and DR/Dt, (vectors) and resulting QR-trajectories (spiralling solid line and dashed separatrix).

7. CONCLUSIONS

The evolution of the invariants of the velocity gradient tensor, Q and R, in the outer layer of a turbulent boundary layer has been studied using a conditional averaging approach. The invariants have been determined from time-resolved 3D experimental (tomographic-PIV) velocity data and are representative of the local flow topology related to the larger scales of motion (>50 viscous length scales).

Both the instantaneous joint-PDF of the invariants and their average temporal behaviour are consistent with previous DNS studies of small-scale motion in isotropic turbulence (Martin et al. 1998, Ooi et al. 1999), at least qualitatively. In the QR phase plane the temporal evolution is characterized by an inward clockwise spiralling trajectory converging to the origin, which translates to the topology around a fluid particle varying cyclic from unstable focus, unstable node, stable node to stable focus, on average. The period of the spiral orbit is nearly constant and determined to be $14.3\delta/U_e$, or $10.4\langle Q_W\rangle^{-1/2}$, in the present flow, which may be regarded as a characteristic lifetime for the eddies in the outer region of the boundary layer ($0.11 < z/\delta < 0.30$). The spatial wavelength length associated to this period is approximately 11δ suggesting a relation with the very large scale motions in the boundary layer as observed in the velocity power spectra (e.g. Balakumar and Adrian 2007, Hutchins and Marusic 2007). Furthermore, some quantitative differences in the orbit's period with respect to the DNS of isotropic turbulence have been observed and discussed.

Inserting the present results into the invariants evolution equations yielded the average effect of the eddy interactions through the pressure and viscous forces. An attempt has been made to model these terms, h_Q and h_R, by data fitting in order to create a simple set of dynamical system equations describing the average evolution of Q and R. This empirical model has been shown to reproduce the main features of the orbits in the QR plane. However, to capture all the detail and improve the accuracy additional, more complex terms will need to be included in the model.

The authors wish to thank F. Scarano, C. Poelma and J. Westerweel from T.U. Delft and A. Schröder and R. Geisler from DLR, Germany, for providing the experimental dataset. The Australian Research Council is gratefully acknowledged for their financial support.

REFERENCES

Adrian, R.J., 2007, "Hairpin vortex organization in wall turbulence," *Phys. Fluids*, Vol. 19, 041301

Blackburn, H.M., Mansour, N.N., and Canttwell, B.J., 1996, "Topology of fine-scale motions in turbulent channel flow," *J. Fluid Mech.*, Vol. 310, pp. 269-292.

Balakumar, B.J. and Adrian, R.J., 2007, "Large- and very large-scale motions in channel and boundary-layer flows," Phil. Trans. R. Soc. A, Vol. 365, pp. 665-681.

Cantwell, B.J., 1981, "Organized motion in turbulent flow," *Ann. Rev. Fluid Mech.*, Vol. 13, pp. 457-515.

Cantwell, B.J., 1992, "Exact solution of a restricted Euler equation for the velocity gradient tensor," *Phys. Fluids A*, Vol. 4, pp. 782-793.

Cantwell, B.J., 1993, "On the behavior of velocity gradient invariants in direct numerical simulation," *Phys. Fluids A*, Vol. 5, pp.2008-2013.

Chong, M.S., Soria, J., Perry, A.E., Chacin, J., Cantwell, B.J. and Na, Y., 1998, "A study of the turbulence structures of wall-bounded shear flows using DNS data," *J. Fluid Mech.*, Vol. 357, pp. 225-248.

Chong, M.S., Perry, A.E. and Cantwell, B.J., 1990, "A general classification of three-dimensional flow fields," *Phys. Fluids A*, Vol. 2, pp. 765-777.

Elsinga, G.E., Scarano, F., Wieneke, B. and Van Oudheusden, B.W., 2006, "Tomographic particle image velocimetry," *Exp. Fluids*, Vol. 41, pp. 933-947.

Hutchins, N. and Marusic, I, 2007, "Evidence of very long meandering features in the logarithmic region of turbulent boundary layers," *J. Fluid Mech.*, Vol. 579, pp. 1-28.

Martin, J., Ooi, A., Chong, M.S. and Soria, J., 1998, "Dynamics of the velocity gradient tensor invariants in isotropic turbulence," *Phys. Fluids*, Vol. 10, pp. 2336-2346.

Ooi, A., Martin, J., Soria, J. and Chong, M.S., 1999, "A study of the evolution and characteristics of the invariants of the velocity-gradient tensor in isotropic turbulence," *J. Fluid Mech.*, Vol. 381, pp. 141-174.

Perry, A.E. and Chong, M.S., 1987, "A description of eddying motions and flow patterns using critical-point concepts." *Ann. Rev. Fluid Mech.*, Vol. 19, pp. 125-155

Schröder, A., Geisler, R., Elsinga, G.E., Scarano, F. and Dierksheide, U, 2008a, "Investigation of a turbulent spot and a tripped turbulent boundary flow using time-resolved tomographic PIV," *Exp. Fluids*, Vol. 44, pp. 305-316.

Schröder, A., Geisler, R., Staack, K., Wieneke, B., Elsinga, G.E., Scarano, F. and Henning, A., 2008b, "Lagrangian and Eulerian views into a turbulent boundary layer flow using time-resolved tomographic PIV," *14th Int. Symp. on Applications of Laser Techniques to Fluid Mechanics*, Lisbon, Portugal.

Soria, J., Sondergaard, R., Cantwell, B.J., Chong, M.S. and Perry, A.E., 1994, "A study of the fine-scale motions of incompressible time-developing mixing layers," *Phys. Fluids*, Vol. 6, pp. 871-884.